Received: 12 February 2021 | Revised: 22 June 2021 | Accepted: 26 August 2021

DOI: 10.1002/hyp.14361

RESEARCH ARTICLE

WILEY

High spatial-resolution monitoring to investigate nitrate export and its drivers in a mesoscale river catchment along an anthropogenic land-cover gradient

Izabela Bujak | Christin Müller | Ralf Merz | Kay Knöller

Department of Catchment Hydrology, Helmholtz Centre for Environmental Research – UFZ, Halle (Saale), Germany

Correspondence
Izabela Bujak, Department of Catchment Hydrology, Helmholtz Centre for Environmental Research - UFZ, Theodor-Lieser Str 4, 06120 Halle (Saale), Germany.
Email: hydrology@izabelabujak.com

Abstract

Nitrate monitoring is commonly conducted with low-spatial resolution, only at the outlet or at a small number of selected locations. As a result, the information about spatial variations in nitrate export and its drivers is scarce. In this study, we present results of high-spatial resolution monitoring conducted between 2012 and 2017 in 65 sub-catchments in an Alpine mesoscale river catchment characterized by a land-use gradient. We combined stable isotope techniques with Bayesian mixing models and geostatistical methods to investigate nitrate export and its main drivers, namely, microbial N turnover processes, land use and hydrological conditions. In the investigated sub-catchments, mean values of NO_3^- concentrations and its isotope signatures ($\delta^{15}N_{NO3}$ and $\delta^{18}O_{NO3}$) varied from 2.6 to 26.7 mg L^{-1}, from −1.3‰ to 13.1‰, and from −0.4‰ to 10.1‰, respectively. In this study, land use was an important driver for nitrate export. Very strong and strong positive correlations were found between percentages of agricultural land cover and $\delta^{15}N_{NO3}$, and NO_3^- concentration, respectively. Mean proportional contributions of NO_3^- sources varied spatially and seasonally, and followed land-use patterns. The mean contribution of manure and sewage was much higher in the catchments characterized by a high percentage of agricultural and urban land cover comparing to forested sub-catchments. Specific NO_3^- loads were strongly correlated with specific discharge and moderately correlated with NO_3^- concentrations. The nitrate isotope and concentration analysis results suggest that nitrate from external sources is stored and accumulated in soil storage pools. Nitrification of reduced nitrogen species in those pools plays the most important role for the N-dynamics in the Erlauf river catchment. Consequently, nitrification of reduced N sources was the main nitrate source except for a number of sub-catchments dominated by agricultural land use. In the Erlauf catchment, denitrification plays only a minor role in controlling NO_3^- export on a regional scale.

KEYWORDS
Bayesian mixing models, informative priors, nitrate isotopes, nitrate pollution, top-kriging

1 | INTRODUCTION

The European Community has been taking measures concerned with nitrate (NO_3^-) water pollution for over 40 years. In 1991, the European Union (EU) introduced the Nitrates Directive, which aimed at reducing water quality deterioration caused by nitrate pollution related to agriculture. Almost 10 years later, in 2000, the EU adopted a Water Framework Directive (EU, 2000) that called for water quality management at the river basins scale. However, despite introducing respective directives and setting up the obligation to develop action plans to prevent nitrate concentrations above 50 mg L^{-1}, many EU countries still exceed this threshold (Schumacher, 2016). Not only EU member states encounter problems related to NO_3^- pollution. Nitrate contamination is a worldwide environmental issue. High NO_3^- concentrations in water threaten not only human health but also the environment as they lead to, among other things, eutrophication and toxic algal blooms (Lee et al., 2008; WHO, 2011). Upper mentioned facts emphasize the importance of a reliable assessment of the interaction between anthropogenic activities and the nitrogen dynamics at the river basins scale. Nevertheless, the basin-scale management approaches in large catchments are hindered due to the poor understanding of the spatial and seasonal variability of nitrate sources, transport and turnover pathways (Lintern et al., 2020). Major uncertainties and knowledge gaps exist with respect to (1) the transport of nitrate from different sources through different compartments of the hydrological system and (2) the degree of transport-related alterations of nitrate source signatures (Lintern et al., 2020; Schlesinger et al., 2006).

A prerequisite for designing effective water pollution mitigation programs is in-depth knowledge of the drivers controlling the spatial and temporal variability in nitrate export at relevant management scales (Wall et al., 2011). Therefore, many researchers addressed the problem of characterization and quantification of nitrate sources and in-stream nitrate processing along with a characterization of its controls (Nestler et al., 2011; Rose et al., 2015; Schwientek et al., 2013). Coupled nitrogen and oxygen stable isotopes of nitrate have proven to be useful to identify nitrate sources and transformations within catchments qualitatively (Xue et al., 2009) not only on a hillslope scale (McAleer et al., 2017) but also in large river basins, such as the Mississippi (Panno et al., 2006), Illinois (Panno et al., 2008), Seine (Sebilo et al., 2006) and Sawa (Vrzel et al., 2016). Stable isotope monitoring in large and mesoscale river catchments is usually conducted at the outlet only or with low-spatial resolution. However, nitrate sources and transformations may display substantial spatial and seasonal variations that can be missed while using traditional, low-spatial resolution monitoring. Moreover, conducting monitoring with a low spatial resolution in large river catchments does not provide insights into how hydrochemical variations at the catchment outlet are linked to the variations in headwater catchments, that are known to be zones of nutrient- and carbon processing (von Schiller et al., 2017) and are recognized for their high ecological value (Bishop et al., 2008; Van Meerveld et al., 2020). Recently, a high spatially resolved investigation of nitrate dynamics has been performed in mesoscale river catchment using coupled dual nitrate isotopes and river discharge (Mueller, Krieg, et al., 2016). The results suggest that such an approach can provide more insights into nitrate dynamics in response to land use and flow regimes.

Stable nitrate isotope signatures coupled with mass balance mixing models were used to quantitatively assess nitrate sources (Deutsch et al., 2006; Voss, Deutsch, et al., 2006). Nevertheless, the usage of mass balance mixing models to trace nitrate sources is constrained to well-defined systems and does not take into account several substantial sources of uncertainties related to (1) multiple nitrate sources, (2) overlapping isotopic compositions of nitrate sources, and (3) the fact that nitrate sources are rarely defined by narrow isotopic ranges. The introduction of the combined usage of Bayesian updating and a Monte Carlo search routine opened new opportunities for tracing sources and the fate of nitrate in river basins. This approach is implemented in programs like SIAR—stable isotope analysis in R (Parnell et al., 2010), and MixSIR (Moore & Semmens, 2008) or the concept of Soulsby et al. (2003). Since first applications of Bayesian stable isotope mixing models (BSIMMs) for estimating the probability distributions of proportional contribution of nitrate sources to the nitrate mixture in surface water (Xue et al., 2012), they have been successfully applied to study nitrate sources under various land uses, including urban (Divers et al., 2014), agricultural (Ding et al., 2014), irrigated (Zhang et al., 2018) and multiple land-use areas (Jin et al., 2018; Li et al., 2019; Xing & Liu, 2016). Advances in the usage of BSIMMs include incorporation of fractionation factors related to denitrification (Li et al., 2019; Xia et al., 2017; Yue et al., 2015) and combination of BSIMM with nitrate export and flux calculations at the catchment outlet in large scale (>350 000 km^2) (Li et al., 2019) or with low-spatial resolution (four locations) in small scale (<16 km^2) (Divers et al., 2014). Moore and Semmens (2008) proposed to improve BSIMMs estimates by the usage of informative prior distributions. To the best of our knowledge, this approach has not yet been used to investigate the contribution of nitrate sources in surface water. Except for that, BSIMMs were not exploited to investigate nitrate export by combining them with nitrate export calculations in high spatial resolution in a mesoscale river basin.

The objectives of this study are to (1) quantitatively determine NO_3^- sources in a mesoscale river catchment with a high spatial resolution, (2) investigate the spatiotemporal variability in mesoscale nitrate export, and (3) to understand how and to what extend different drivers shape nitrate export from a mesoscale catchment. Our key research hypothesis is that nitrate export from mesoscale river catchments is predominantly controlled by land use, while hydro-climatic forcing and microbial N-turnover processes play a secondary role. Furthermore, we hypothesize that nitrification of reduced nitrogen stored in the soil compartment is an important nitrate source on larger scales, especially during periods of higher hydrological activity. The novelty of this study is the approach we used to test this hypothesis. Our approach integrates spatially highly resolved stable isotope and hydrochemical monitoring with high-resolution discharge data obtained by the geostatistical top-kriging method and a Bayesian mixing model with informative priors. The approach aims to better capture the highly dynamic spatiotemporal patterns of nitrate export

and its drivers in the mesoscale river catchments. The approach is applied to a mesoscale Alpine foothill catchment with a land-use gradient, where monitoring data of 19 sampling campaigns conducted between 2012 and 2017 at in total of 65 locations are available. The monitoring data involves various sub-catchments at different seasons and hydrological conditions.

2 | MATERIALS AND METHODS

2.1 | Study area

The Erlauf catchment, with a total catchment area of 631.5 km^2 (BMLFUW, 2014), is situated in Alpine foothills in Austria (Figure 1). The 68 km long river Erlauf is a tributary of the Danube (Braun & Schagerl, 2010). The altitude range of the catchment is from ca. 1900 m a.s.l. at headwaters to ca. 210 m a.s.l. at the river mouth. The investigated catchment is part of the Northern Calcareous Alps, where karst phenomena are known to occur. Carbonate rocks, such as limestone, dolomite, marl, and marlstone are common, especially in the Southern part of the catchment (Strauss, 2009). Besides carbonate rocks, clay, claystone, sand, sandstone, gravel, slate, and coal are also present (GBA, 2020). We used the CORINE Land Cover dataset (EEA, 2012) to perform the land use analysis. The forest and the semi-natural areas made up 51% of the catchment area. Agricultural areas occupy 34% of the catchment, including 15% of pastures and 10% of the non-irrigated arable land. Water bodies encompass 12% of the total catchment area. In the southern part of the catchment, three major lakes are located: Erlauf lake (0.56 km^2), Erlauf water reservoir (0.3 km^2), and Lassing water reservoir (0.1 km^2) (BMLFUW, 2014). Artificial surfaces account only for 3%. In the Erlauf basin, there are five wastewater treatment plants (OIEau, 2019) (Figure 1). In the Northern part of the catchment (location B4), the input of nitrogen fertilizer ranged from 140 kg N ha^{-1} (2013) to 210 kg N ha^{-1} (2012) between the years 2010–2013 (Blöschl et al., 2016). The crops are mainly maize, winter wheat, rape, and barley. We determined the sub-catchment size for each sampling location based on the LiDAR digital elevation model (Land Kärnten, 2015) with a resolution of 10 m and the exact sampling location. Subsequently, we calculated the percentage of the main land cover types for each sub-catchment, namely, forest (LC_{FOR}), agricultural areas (LC_{AGR}), and urban areas (LC_{URB}). For the computations, we used the software ArcGIS version 10.4 and the Zonal Statistics Tool. The mean discharge of 14.6 m^3 s^{-1} has been observed at the gauging station located close to the outlet (Niederndorf) (NÖ, 2019). Between the years 2014 and 2018, the mean annual precipitation varied from 1922 mm in the mountainous region (the gauging station in Wastl am Wald) to 768 mm in the lowlands (the gauging station in Wieselburg) (NÖ, 2019). There is no clear seasonality in the precipitation at the catchment scale. However, precipitation in the lowland is higher in summer compared to the rest of the year (Figure S1).

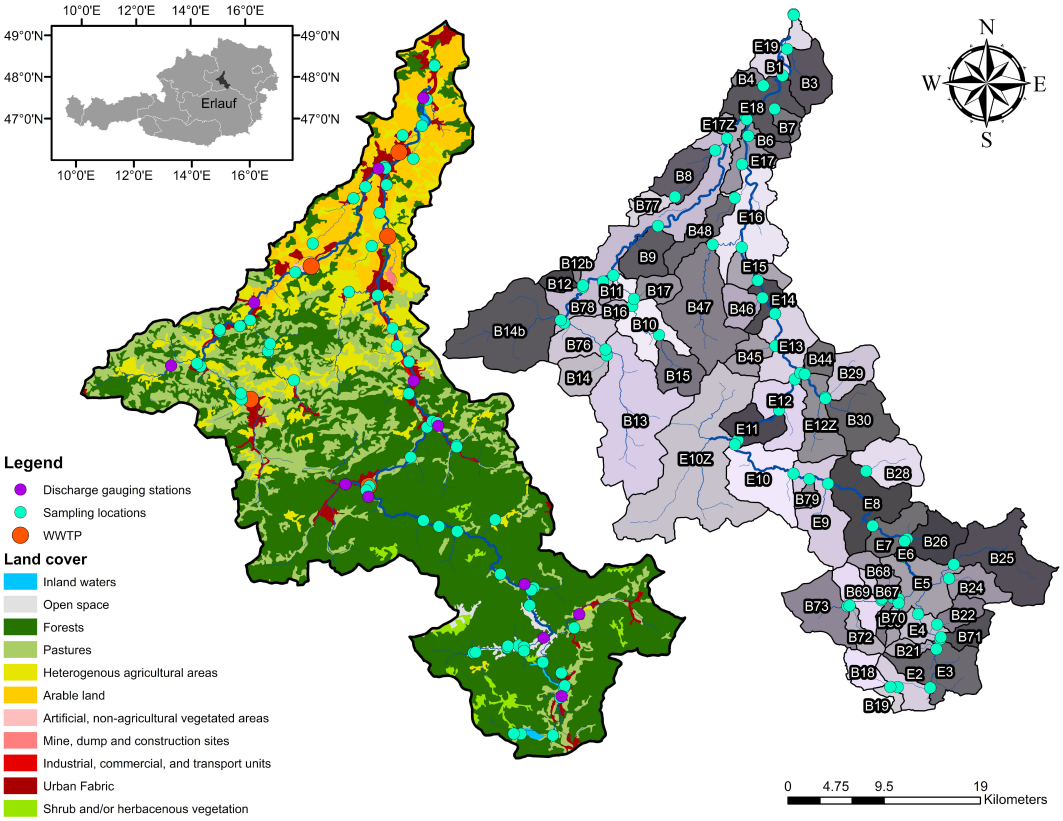

FIGURE 1 Map of the Erlauf catchment and its tributaries with land cover (left) and all surface water sampling locations monitored from 2012 to 2018, each representing sub-catchment (right). WWTP states for wastewater treatment plants

2.2 | Sampling

We conducted our monitoring program in the Erlauf catchment between 2012 and 2017. Our sampling methodology involved a combination of regional and event-based surface water sampling campaigns. We performed regional sampling campaigns seasonally with a high spatial resolution, including the main river and all its major tributaries. Regional sampling campaigns were complemented by four event-based (event-triggered) sampling campaigns conducted at selected sampling locations. We carried out event-based campaigns during or immediately after precipitation events no more than 3 days after scheduled regional sampling campaigns. Altogether, we performed 19 surface water sampling campaigns and monitored 65 sampling locations. The details regarding the dates and locations of the surface water monitoring are provided in the supplementary information (Table S1). Regional sampling campaigns were performed generally during base flow conditions with daily average precipitation during campaigns not exceeding a few mm (Table S2, and Figure S2). However, conditions antecedent to regional sampling campaigns were variable (Table S2), resulting in varying average discharges calculated at the outlet for the regional sampling campaigns (Table S2).

At each site, using the portable meter, we measured the basic physicochemical properties of water, including electrical conductivity (EC), temperature (T), and pH. Furthermore, we collected water samples for major ion and stable isotope analysis of nitrate and water. All samples were kept in high-density polyethene (HDPE) bottles without headspace. Besides the surface water monitoring, we collected precipitation samples of rainfall and snow in the study catchment. Precipitation water was collected as monthly composite samples in evaporation-free precipitation collectors (PALMEX, Croatia; Gröning et al., 2012) with a volume ranging from 30 ml to 2.5 L. Additionally, we collected 1 L snow grab samples during winter. In total, 61 precipitation samples and 691 stream water samples were collected and analysed for nitrate and water stable isotopes, as well as nitrate concentrations.

2.3 | Laboratory analysis

Water samples for stable isotope and chemical analysis were filtered through cellulose acetate filters with a pore size of 0.22 and 0.45 μm, respectively. Samples were stored refrigerated prior to analysis within 1 month of collection. The denitrifier method with bacteria strains of *Pseudomonas chlororaphis* (ATCC #13985) was used to measure the isotopic composition of dissolved nitrate (Casciotti et al., 2002; Sigman et al., 2001). The isotopic composition of N_2O ($\delta^{15}N_{NO3}$ and $\delta^{18}O_{NO3}$) produced from sample NO_3^- was measured by gas isotope ratio mass spectrometry. A DELTA V Plus mass spectrometer, in combination with a GasBench II from Thermo Scientific, was used for the nitrate isotope determination. Stable isotope ratios are expressed in the delta (δ) notation as follows: (Kohl et al., 1971):

$$\delta(‰) = \left(\frac{R_{sample}}{R_{standard}} - 1\right) \times 1000(‰), \quad (1)$$

where R_{sample} and $R_{standard}$ are the sample's and the standard's ratio of the heavier to the lighter isotope. The $\delta^{15}N_{NO3}$ values are reported relative to the atmospheric nitrogen, and $\delta^{18}O_{NO3}$ are reported relative to the Vienna Standard Mean Ocean Water (VSMOW). The SDs for the nitrogen and the oxygen isotope measurements of nitrate are ±0.4‰ and ± 1.6‰, respectively. The following international standards were used for calibration: USGS32, USGS34, USGS35 and IAEA NO3. Moreover, all samples were analysed for stable isotopes of water (δ^2H_{H2O} and $\delta^{18}O_{H2O}$) by laser cavity ring-down spectroscopy (L2120-I, Picarro Inc.). The analytical precision of the method is 0.8‰ and 0.1‰ for δ^2H and $\delta^{18}O$, respectively. Stable isotopes of water are reported relative to the international standard VSMOW. Anions (Cl−, and NO_3^-) were analysed using ion chromatography (IC).

2.4 | Determination of potential nitrate sources and their chemical and isotopic composition

Based on the land use characteristics, we determined four potential sources of riverine NO_3^- in the study area, that is, atmospheric deposition (AD), nitrate fertilizers (NF), manure and sewage (MS), and nitrification of reduced N sources (RNS). The RNS source consists of NO_3^- derived from nitrification of nitrogen originating in several other sources, namely, soil organic matter, mineral fertilizers (except nitrate salts), and ammonium in precipitation. The values of these sources overlapped to such an extent that distinguishing among them without an additional tracer would be questionable.

To estimate the proportional contribution of the four potential NO_3^- sources, the typical nitrate isotopic signatures of those sources have to be known, that is, mean $\delta^{15}N_{NO3}$ and $\delta^{18}O_{NO3}$ values as well as their SDs. Means and SDs of $\delta^{15}N_{NO3}$ and $\delta^{18}O_{NO3}$ of atmospheric deposition (AD) were based on isotopic signatures measured from the precipitation samples that we collected in the study area between 2012 and 2017. The oxygen isotope signatures of the same precipitation samples were used to calculate means and SDs of $\delta^{18}O_{NO3}$ of RNS and MS, assuming that NO_3^- is formed by microbial nitrification (Text S1). We compiled the data available in relevant literature to obtain means and standard deviations of $\delta^{15}N_{NO3}$ of RNS, MS, and NF and $\delta^{18}O_{NO3}$ of NF (Bateman & Kelly, 2007; Curt et al., 2004; Fogg et al., 1998; Heaton, 1986; Kreitler & Browning, 1983; Li et al., 2007; Mariotti et al., 1988; Mayer et al., 2001; Panno et al., 2008; Rapisarda et al., 2010; Rennie et al., 1976; Rogers, 2008; Spoelstra et al., 2007; Vitòria et al., 2004; Wassenaar, 1995; Widory et al., 2005; Williard et al., 2001; Zhang et al., 2008). We have described in detail the procedure of calculating the mean isotopic signatures of nitrate sources in the supplementary information (Text S1).

We used NO_3^- /Cl^- molar ratios as an indicator of nitrate sources since different NO_3^- sources have different levels of NO_3^- /Cl^- ratios. The mineral fertilizers are characterized by high NO_3^- /Cl^- molar ratios and low concentrations of Cl^-, while untreated effluents from MS have relatively low NO_3^-/Cl^- ratios and high Cl^- concentrations (Liu et al., 2006). The NO_3^-/Cl^- ratios of sewage will increase after being treated in wastewater treatment plants (Xia

et al., 2017). In the Erlauf watershed, neither halite nor sylvite deposits occur. Therefore, we expect no influence of evaporites on NO_3^-/Cl^- ratios.

2.5 | Stable isotope mixing model

We used MixSIAR, a Bayesian tracer (e.g. stable isotope) mixing model framework (Moore & Semmens, 2008; Parnell et al., 2010; Stock et al., 2018), to calculate the proportional contribution of NO_3^- sources in surface water in all sub-catchments. Supplementary Information (Text S2) includes additional information about the model.

2.6 | Discharge and precipitation data

The daily discharge data were provided by the state government office of Lower Austria ('Amt der Niederösterreich Landesregierung'). In the Erlauf catchment, there are 12 gauging stations. Five of them are located along the main river, and the other seven are on the main tributaries (Figure 1).

Daily precipitation data were obtained for eight stations located within the catchment and in the close neighbourhood (Table S3) from the web page of the state government office of Lower Austria (NÖ, 2019).

2.7 | Regionalization of river discharge and nitrate loads

To calculate the nitrate export from all investigated sub-catchments and to understand the spatial heterogeneity of the nitrate export and its controls, we interpolated the runoff in our sampling locations from discharge gauging stations on a daily time step using the top-kriging technique. Top-kriging, developed by Skøien et al. (2006), is a geostatistical method that allows interpolating runoff characteristics along with the stream network. In comparison to traditional deterministic or geostatistical interpolation approaches, it accounts for the river network hierarchy. More details can be found in Skøien and Blöschl (2007).

As the regional sampling campaigns were conducted within 4 days during steady flow conditions with only small intra-campaign changes in discharge, and the event-based sampling campaigns were conducted within a one-time step, discharge variability due to the travel time of the event wave between up- and downward river cross-sections is assumed to be small. Therefore, we used spatial kriging (time-independent kriging). We leveraged the rtop package (Skøien et al., 2014) in the statistical environment R (R Core Team, 2018) to apply the top-kriging approach. We tested the predictive accuracy of the interpolation using ordinary cross-validation. In the ordinary cross-validation, each gauged station is, in turn, treated as an ungagged station, and the runoff is interpolated from the other gauged stations. The interpolated runoff is then compared with the observed daily runoff. We quantified the predictive accuracy with the Nash–Sutcliffe Efficiency (NSE) (Nash & Sutcliffe, 1970). As a result of our calculations, we obtained the mean NSE at the level of 0.86. The high cross-validation NSE values indicate that the top-kriging regionalization captures well the observed local runoff dynamics. NSE values are also in the range of cross-validated NSE values of Parajka et al. (2015) using a well-established variogram fitted to several hundred runoff stations in Austria (Merz et al., 2008; Skøien et al., 2006). Previous studies (Lark, 2000; Skøien et al., 2014) show that the quality of the predictions is relatively insensitive to the choice of the variogram, at least as long as there are several observations within its range. In the Erlauf catchment, a high density of stations (12 stations per 631.5 km^2) is available.

We calculated the specific discharge (Q_{spec}) by dividing the discharge by the respective catchment area. Subsequently, we calculated the nitrate loads (L_{NO3}) and specific nitrate loads (SL_{NO3}) for each sampling point and each campaign. We calculated L_{NO3} by multiplying measured nitrate concentrations with the average discharge of the sampling campaign. Specific nitrate loads were calculated by dividing calculated nitrate loads by the respective catchment areas.

2.8 | NO_3^- loads derived from different sources

For each sub-catchment, in turn, we calculated what portion of the NO_3^- load was derived from each of the four sources (AD, NF, RNS, and MS). We did it by multiplying the SL_{NO3} calculated for a specific sampling campaign (Section 2.7) with the mean contribution of each of the four NO_3^- sources calculated for the respective sub-catchment (Section 2.5). For this analysis, we selected five seasonal sampling campaigns conducted from April 2013 to January 2014. Event-based sampling campaigns were not included in this analysis. All five selected sampling campaigns were performed during different months, with the average discharge calculated at the river outlet of 20.4, 19.3, 6.8, 7.4 and 6.7 $m^3\ s^{1-}$, for the sampling campaigns performed in April, June, August, November, and January, respectively.

2.9 | Discharge separation

To shed more light on the dynamics of hydrological processes, we divided streamflow into the base flow and quick flow components. The contribution of these components is likely to affect nitrate concentrations and isotopic compositions because various pathways for the mobilization of nitrogen from natural and anthropogenic sources may be associated with certain hydrological events. Therefore, we conducted a separation of total discharge with a simple smoothing method proposed by the Institute of Hydrology (1980) at all locations (Text S3). Based on discharge separation, we calculated the base flow index (BFI), defined as a ratio of base flow to total flow. We did it separately for all sampling locations and each sampling campaign. If sampling campaigns lasted longer than 1 day, we used the average BFI value for all sampling days of the respective campaign.

2.10 | Other statistics and calculations

We applied the one-way repeated analysis of variance (repeated ANOVA) with a subsequent pairwise *t*-test to test the differences in $\delta^{15}N_{NO3}$ and $\delta^{18}O_{NO3}$ between all seasons. To test the differences in NO_3^- concentrations, the Friedman test with subsequent pairwise Wilcoxon test was applied. Moreover, for each sampling location, we calculated the correlation matrix of pairwise contributions of all variables based on Spearman's correlation coefficient and Pearson's correlation coefficient. We tested the differences in NO_3^- concentrations, $\delta^{15}N_{NO3}$, $\delta^{18}O_{NO3}$, and $\delta^{18}O_{H2O}$ between pre-event and event-based sampling campaigns using the Wilcoxon test. Moreover, we calculated Spearman's correlation rank and Pearson correlation coefficient between BFI and $\delta^{18}O_{NO3}$ for all sub-catchments that were sampled at least 10 times, in turn.

To investigate the potential impact of denitrification, we performed a location-wise and spatial analysis. In the location-wise analysis, we firstly included data from all sampling campaigns. In this analysis, we calculated the linear regression between $\delta^{18}O_{NO3}$ and $\delta^{15}N_{NO3}$, as well as between $\delta^{15}N_{NO3}$ and the natural logarithm of NO_3^- for all sub-catchments. Secondly, we investigated inter-campaign variations by examining changes of nitrate isotope signatures and nitrate concentrations occurring at the same sampling location between two subsequent seasonal sampling campaigns. To declare that a sampling location was potentially affected by denitrification, we verified if the following conditions are met (1) a simultaneous increase in $\delta^{15}N$ and $\delta^{18}O$ with a slope between 1:1.3 and 1:2.1, and (2) a decrease in NO_3^- concentrations larger than 0.2 mg L^{-1}. Likewise, to obtain spatial information on the potential impact of denitrification, we analysed the changes in $\delta^{18}O_{NO3}$, $\delta^{15}N_{NO3}$ and NO_3^- along the main river.

The field-based, apparent enrichment factors for nitrogen ($^{15}\varepsilon$) and oxygen ($^{18}\varepsilon$) were calculated using the simplified Rayleigh equation:

$$\varepsilon = \frac{(\delta - \delta_{\text{initial}})}{\ln\left(\frac{C}{C_{\text{initial}}}\right)}, \quad (2)$$

where ε stands for the isotopic enrichment factors for nitrogen and oxygen, d stands for the $\delta^{15}N$ and $\delta^{18}O$ values, respectively, and C stands for the nitrate concentration.

3 | RESULTS

3.1 | Qualitative determination of nitrate sources

Figure 2 presents the means and SDs of four potential nitrate sources in the study area, as well as the isotopic signatures of all surface water and precipitation samples collected in the study area. For the Erlauf River, the calculated mean $\delta^{18}O_{NO3}$ expected from nitrification (see Section 3.1) is −0.3‰ (±4.0‰) with the minimum of −9.0‰, and the maximum of 8.2‰.

The ratios of NO_3^-/Cl^- varied widely from 0.12 to 14.06 in the catchment, suggesting a mixture of multiple sources of nitrate. In general, high Cl^- concentrations and low NO_3^-/Cl^- ratios were found in catchments with a high percentage of agricultural land use. This could be caused by the high contribution of manure and effluents from sewage. Contrary, low Cl^- concentrations and a wide range of NO_3^-/Cl^- ratios were found in catchments with a low percentage of agricultural land use, reflecting the impact from atmospheric deposition and RNS (Figure S4).

3.2 | Spatiotemporal variations of nitrate isotopes and concentrations in stream water

3.2.1 | Spatial variability

Spatially, mean NO_3^- concentrations from respective sub-catchments ranged from 2.6 to 26.7 mg L^{-1}, while standard deviations varied between 0.6 to 14.5 mg L^{-1} (Figure 3). Generally, mean NO_3^- concentrations and their standard deviations increased from the upper reaches in the spring area to the lower reaches in the agricultural lowlands.

Mean $\delta^{15}N_{NO3}$ ranged from −1.3‰ to 13.1‰, while SDs varied between 0.6‰ and 3.9‰. In general, high mean $\delta^{15}N_{NO3}$ values were found in small sub-catchments in agricultural lowlands, while the lowest mean $\delta^{15}N_{NO3}$ values were found in the southern forested sub-catchments. The $\delta^{15}N_{NO3}$ SDs did not follow the same pattern. The

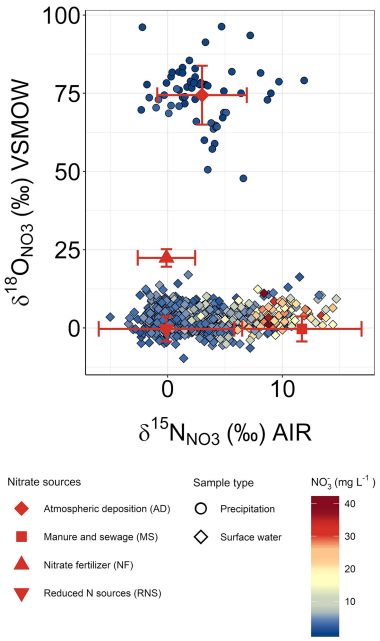

FIGURE 2 The iso-space plot of all samples collected during the monitoring of the Erlauf River catchment in the years 2012 to 2018. Red figures present the calculated means and whiskers represent standard deviations of all potential nitrate sources. Dual isotope plots of surface water samples collected in different seasons are shown in SI, Figure S3

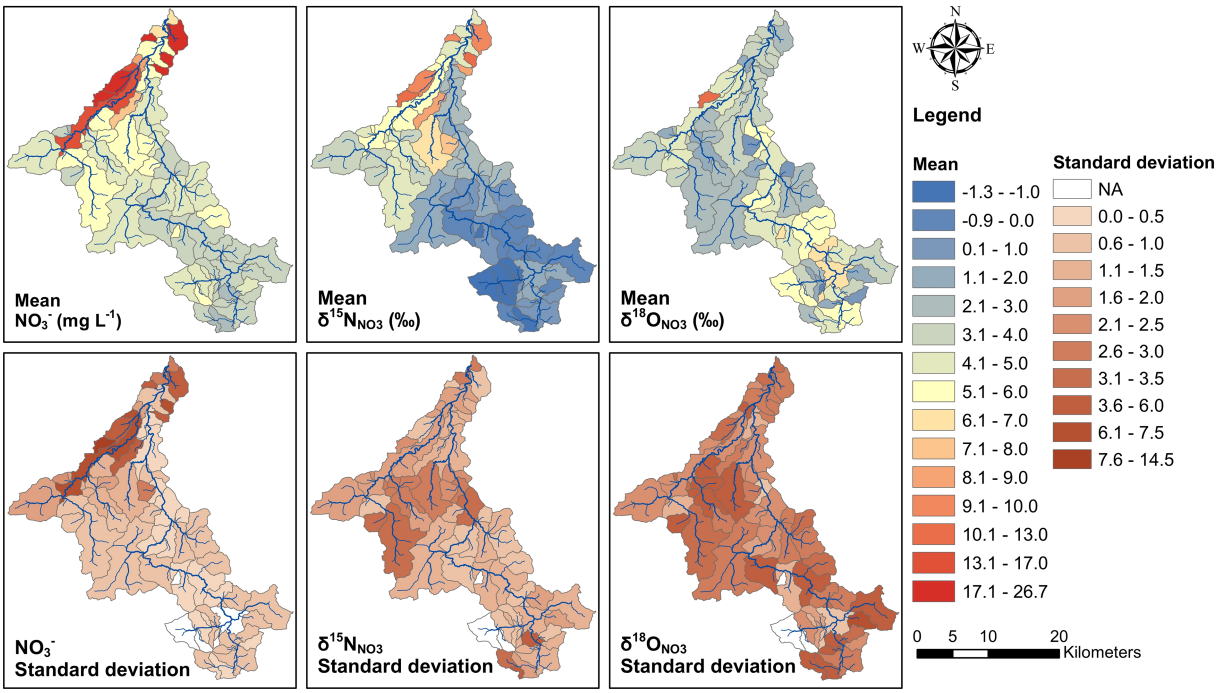

FIGURE 3 Spatial variations of mean NO_3^- concentrations and isotope signatures (upper row) with corresponding standard deviations (lower row)

highest values were found in the central part of the catchment and two locations in the southern part (spring and Erlauf water reservoir).

Mean $\delta^{18}O_{NO3}$ ranged from −0.4‰ to 10.1‰ while SDs varied between 1.0‰ and 7.7‰. Generally, mean $\delta^{18}O_{NO3}$ and their standard deviations were spatially variable.

3.2.2 | Temporal variability

We investigated the temporal variations of NO_3^- concentrations and stable isotope signatures on a seasonal basis. We observed a significant difference in $\delta^{15}N_{NO3}$ between April and all other months (Figure 4a). Similarly, we observed a significant difference between samples collected in November and the other months for $\delta^{18}O_{NO3}$ (Figure 4b). We detected a significant difference in NO_3^- concentrations between samples collected in April and samples collected in December or January (Figure 4c). We found the highest coefficient of variation in June (102%) and the lowest in April (88%).

3.3 | Correlation analysis

Results of the pairwise Spearman's correlation analysis of all collected surface water samples (Figure 5) show that LC_{AGR} and LC_{FOR} were very strongly correlated with $\delta^{15}N_{NO3}$ and strongly correlated with NO_3^- concentrations. Moreover, we found a moderate positive correlation between NO_3^- concentrations and $\delta^{15}N_{NO3}$. Contrary, LC_{AGR} and LC_{FOR} were very weakly correlated with $\delta^{18}O_{NO3}$. Q_{spec} was weakly correlated with stable isotope signatures and very weakly correlated with NO_3^- concentrations. We found a very weak correlation between NO_3^- concentrations and $\delta^{18}O_{NO3}$. SL_{NO3} was strongly correlated with Q_{spec} and moderately correlated with NO_3^- concentrations. Generally, we found higher SL_{NO3} in catchments with higher LC_{AGR}. Even though LC_{AGR} and LC_{FOR} were strongly correlated with NO_3^- concentrations, the correlations between SL_{NO3} and LC_{AGR} or LC_{FOR} were only weak.

All sub-catchments show a negative dependency of BFI and $\delta^{18}O_{NO3}$, of which one-fifth has a very strong or strong correlation (Table S6). A similar general tendency was observed neither between BFI and $\delta^{15}N_{NO3}$ nor between BFI and NO_3^- concentrations.

The analysis of the relationship between nitrogen and oxygen isotope signatures of nitrate on a seasonal basis (Figure S3) shows no positive linear correlation with a slope from 1:1.3 to 1:2.1. During the location-wise analysis of data from all sampling campaigns (see Section 2.10), 60 out of 62 analysed locations did not show significant linear regressions specific for denitrification (Table S4). Nine sets of sampling campaigns (Table S5) matched the prerequisites of inter-campaign analysis (see Section 2.10). For those nine sets, calculated $^{15}\varepsilon$ ranged from −6 to −46 while $^{18}\varepsilon$ ranged from −8 to −69 (Table S5). Spatial analysis along the main river shows that increased isotopic signatures were generally accompanied by increased nitrate concentrations and nitrate loads (Figure S7).

3.4 | Spatiotemporal variations of nitrate sources and loads

The model output (Figure 6) shows that calculated probability distributions of nitrate source contributions differ mainly between the

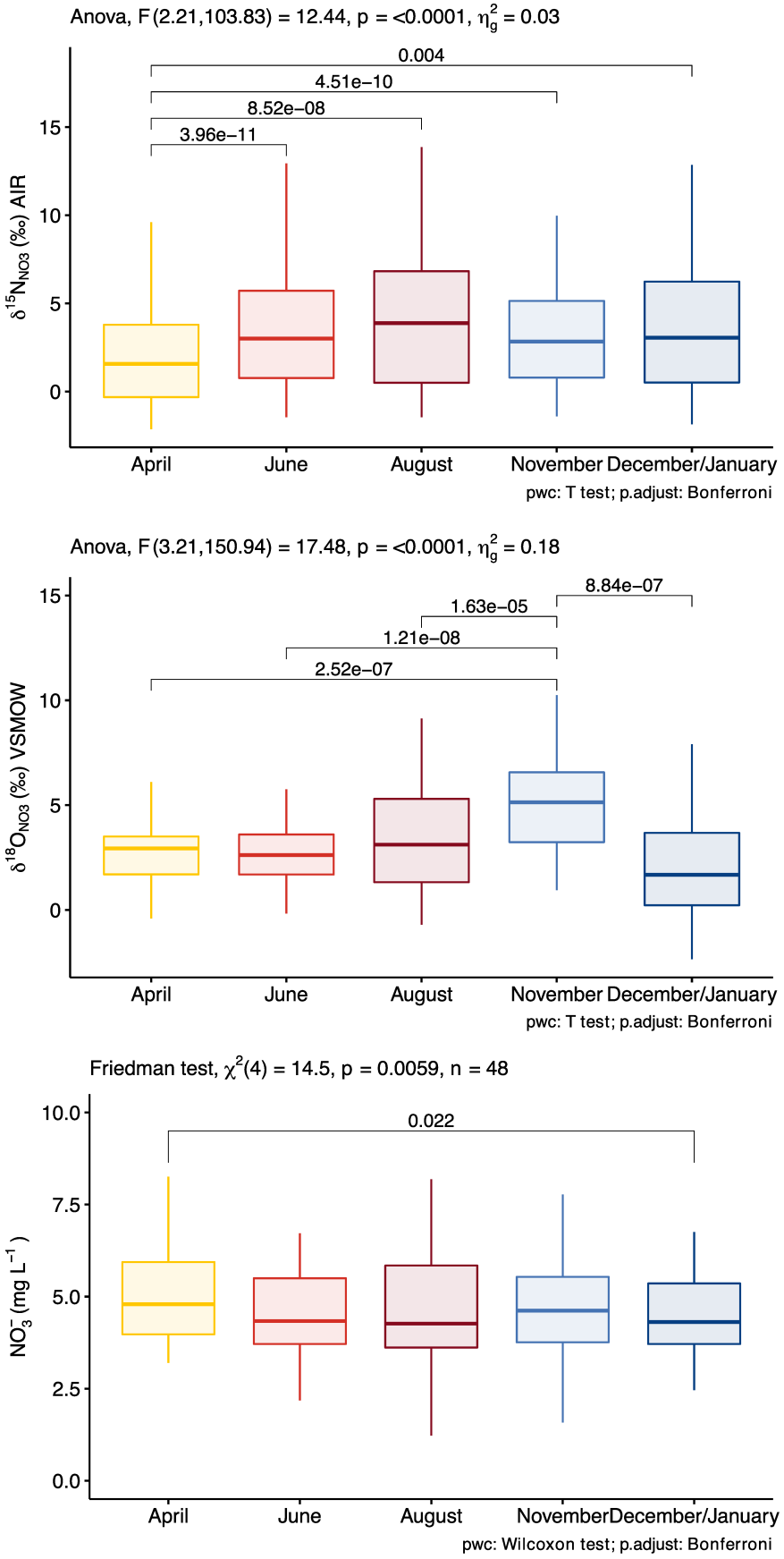

FIGURE 4 Temporal variations of NO_3^- concentrations, and stable isotope signatures in the Erlauf catchment, together with results of repeated analysis of variance, Friedman test, and the pairwise comparisons among different months. Error bars represent standard deviation

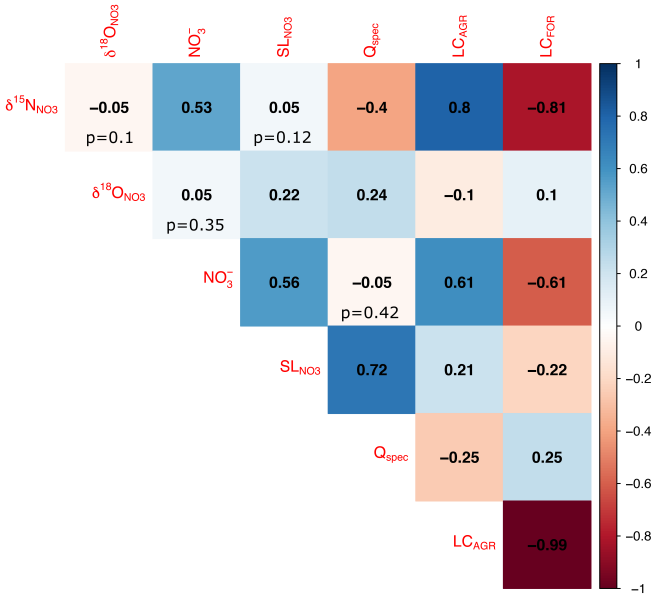

FIGURE 5 The spearman pairwise correlation matrix between nitrate isotopes signatures ($\delta^{15}N_{NO3}$, and $\delta^{18}O_{NO3}$), nitrate concentrations (NO_3^-), specific nitrate loads (SL_{NO3}), specific discharges (Q_{spec}), and percentages of the agricultural (LC_{AGR}) and the forested land cover (LC_{FOR}), based on all samples collected from all sampling locations. Correlations with the *p* value >0.001 are specified on the plot

different land-use areas, but seasonal differences are also visible (Text S4). In the Erlauf spring area (headwater sub-catchment B18, 2.7 km^2, with 99.7% forest, and 0.3% agriculture), the primary source of NO_3^- calculated for the whole monitoring period was RNS with the mean contribution of 95%, followed by AD (5%), and the contribution of two other sources close to zero. At the outlet of the river (location E19), the primary source of NO_3^- calculated for the whole monitoring period was also RNS with the mean contribution of 46%, followed by MS (44%), NF (8%), and AD (2%). In the sub-catchment characterized by the highest percentage of agriculture (location B7; 3 km^2, with 100% of agricultural areas), the primary source of NO_3^- calculated for the whole monitoring period was MS with the mean contribution of 83%, followed by NF (9%), RNS (6%), and AD (3%).

We found the highest SL_{NO3} in April and June (Figure 7, columns 1 and 2). During all analysed months, SL_{NO3} were generally increasing from south to north. We found the highest SL_{NO3} in small agricultural sub-catchments with a high percentage of arable land located next to the Erlauf river outlet. The analysis of the SL_{NO3} derived from each of the four sources (Figure 7, rows 2–5) reveals that in those catchments higher total SL_{NO3} were caused mainly by increased SL_{NO3} derived from MS. Generally, the SL_{NO3} were higher in catchments characterized by higher LC_{AGR}, especially those characterized by a high percentage of arable land. The SL_{NO3} derived from AD were very low. The SL_{NO3} derived from RNS did not follow a spatial pattern and were highest in April and June. The SL_{NO3} derived from NF were highest in April and June, especially in catchments with a high percentage of arable land.

3.5 | Event-based monitoring

We did not observe any significant difference in mean NO_3^- concentrations nor mean $\delta^{15}N_{NO3}$ between pre-event and event-based sampling campaigns (Table 1). For winter and spring event-based sampling campaigns, we observed a significant difference in mean $\delta^{18}O_{NO3}$ and $\delta^{18}O_{H2O}$ in comparison to the values measured during antecedent pre-event sampling campaigns, with *p* values lower than 0.001 and 0.05, respectively. During summer and autumn rainfall-runoff events, we neither detected a significant difference for $\delta^{18}O_{NO3}$ nor $\delta^{18}O_{H2O}$.

We identified moderate to strong positive linear correlations between the LC_{AGR} and the difference between $\delta^{15}N_{NO3}$ measured during pre-event and event sampling campaigns in the respective sub-catchments for three out of four investigated events (Figure 8). Accordingly, the difference in $^{15}N_{NO3}$ is negatively correlated to the LC_{FOR}. A similar strong correlation was neither found between the LC_{AGR} and change in $\delta^{18}O_{NO3}$ nor between LC_{AGR} and change in NO_3^- concentrations (Table S7). For the autumn event, no correlation between the LC_{AGR} and the difference between $\delta^{15}N_{NO3}$ measured during a pre-event and event sampling campaign was observed (Figure 8d).

4 | DISCUSSION

4.1 | Dynamics of NO_3^- export and microbiological NO_3^- transformations

Nitrification and denitrification processes are important steps in the nitrogen cycle that govern N loss and N_2O emissions. Because they imprint a traceable change in nitrate stable isotope signatures, stable isotopes of nitrate can be used to get insights into these drivers.

Denitrification produces simultaneously enriched dual isotopic values of nitrate in combination with decreasing nitrate concentrations. In theory, $\delta^{15}N_{NO3}$ plotted against the natural logarithm of NO_3^- concentration should yield a straight line. Previous studies noted that a positive linear relationship between $\delta^{15}N_{NO3}$ and $\delta^{18}O_{NO3}$, with a slope from 1:1.3 to 1:2.1, is characteristic for denitrification (Aravena & Robertson, 1998; Fukada et al., 2003; Mengis et al., 1999). The analysis of the relationship between nitrogen and oxygen isotope signatures of nitrate on a seasonal basis does not provide any evidence for a strong impact of denitrification (Figure S3). During the location-wise analysis of data from all sampling campaigns, most locations did not show significant linear regressions specific for denitrification (Table S4). However, two sampling locations displayed slopes in the dual-isotope plot that might be indicative of the occurrence of denitrification with weak correlations. Their further analysis showed that the correlation between $\delta^{18}O_{NO3}$ and $\delta^{15}N_{NO3}$ in one of the locations is driven rather by the mixing of different sources than denitrification (Figure S5). However, the possibility of a weak denitrification signal could not be rejected in the second location (Figure S6). Nevertheless, on average, less than 0.6% of the nitrate load at the outlet of the Erlauf River is delivered from this location. Therefore, even if denitrification occurred in this location, it had a negligible impact on the isotopic composition of the

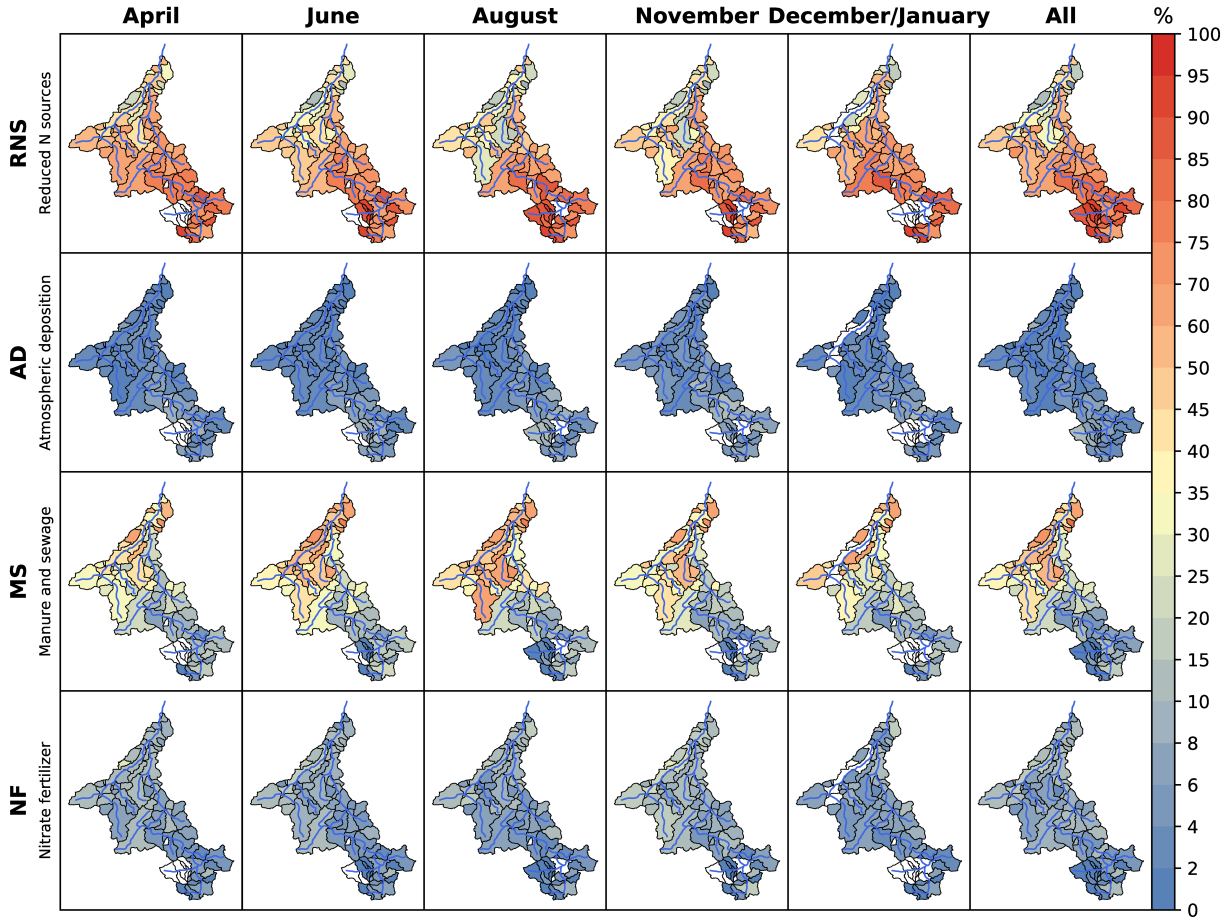

FIGURE 6 Proportional contributions of four potential NO_3^- sources estimated by the MixSIAR model are presented for all sub-catchments seasonally and for all collected data (last row). White colour refers to a lack of data (Table S1)

main river. The location-wise analysis of data from all sampling campaigns did not provide any evidence for a significant role of denitrification in nitrate turnover on the entire river system. Previous research has shown that denitrification may occur in so-called hot spots and hot moments when conditions are favourable (e.g. Harms & Grimm, 2008; Palta et al., 2014; Peter et al., 2011). Therefore, we performed further inter-campaign analyses (see Section 2.10), during which nine sets of sampling campaigns (Table S5) matched the prerequisites. However, except for one location, subsequent analysis of $^{15}\varepsilon$ and $^{18}\varepsilon$ (Table S5) did not confirm straightforward denitrification as the sole process controlling the isotopic composition of nitrate. The $^{15}\varepsilon$ of denitrification reported in the literature vary between −40‰ and −5‰ (Kendall & McDonnell, 1998) with typical values reported for groundwater denitrification between −8‰ and −5‰ (Mariotti et al., 1988). The oxygen isotope enrichment factors for denitrification ($^{18}\varepsilon$) fall between −18‰ and −8‰ (Xue et al., 2009). The apparent enrichment factors calculated based on Equation (2), were lower than the typical range of $^{15}\varepsilon$ for denitrification. Moreover, all occasions of the inter-campaign analysis where results gave some indication for the impact of denitrification had relatively low isotopic signatures, with $\delta^{18}O_{NO3}$ not exceeding the typical range for nitrification. Further spatial analysis along the main river did not show a considerable impact of bacterial denitrification (Figure S7).

While a considerable portion of the measured surface water $\delta^{18}O_{NO3}$ values (61%) fell into the range of the standard deviation from the mean estimated value, over 91% of all measured surface water $\delta^{18}O_{NO3}$ values plot in the range between minimum and maximum estimated value for $\delta^{18}O$ of nitrate derived from nitrification (Figure 2). The facts mentioned above indicate the dominance of the nitrification process for controlling the N-dynamics in the Erlauf basin. 9% of samples have $\delta^{18}O_{NO3}$ higher than theoretically expected for nitrification-derived nitrate what is likely caused by the enriched residual water $\delta^{18}O_{H2O}$ due to (1) a higher fractionation by respiration in soil (Kendall et al., 2007; Mayer et al., 2001), (2) a higher exchange of oxygen atoms between intermediate N-compounds (nitrite) and water (Casciotti & Buchwald, 2012; Kool et al., 2011), or higher evaporation causing a positive water oxygen isotope shift.

Overall, our analyses showed that nitrate concentrations are likely to be controlled by nitrification processes. On a regional scale, bacterial denitrification plays only a minor role in the Erlauf catchment. Previous studies used stable isotopes to evaluate large-scale patterns in N turnover processes showing that they can be variable and site-specific. Denitrification was found to have a negligible impact on a regional scale nitrate turnover in Bode catchment characterized with similar land use and topographic gradients (Mueller, Krieg, et al., 2016; Mueller, Zink, et al., 2016). Dual isotope evaluation of nitrate proved

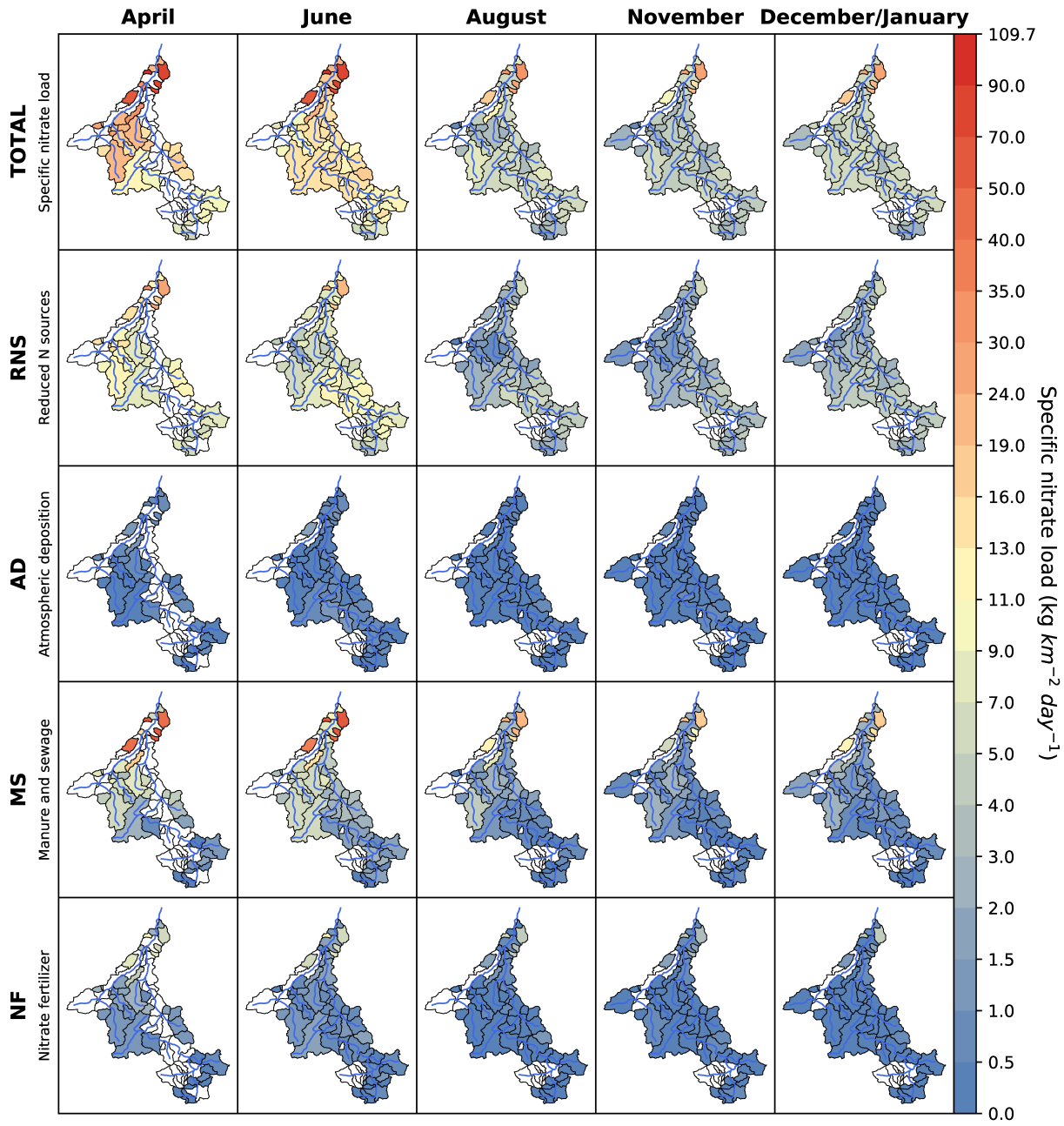

FIGURE 7 Row 1 (top) presents specific NO_3^- loads (SL_{NO3}) calculated for each sub-catchment, and rows 2 to 5 present SL_{NO3} derived from each of four NO_3^- sources. In the figure presented are SL_{NO3} calculated for five selected seasonal sampling campaigns from April 2013 to January 2014, based on NO_3^- concentrations measured during respective sampling campaign, discharge data calculated by the usage of the top-kriging (Section 2.7), and mean NO_3^- sources contributions calculated by the usage of MixSIAR (Figure 6, columns 1 to 5, respectively). White colour refers to a lack of data (Table S1)

that denitrification was a main regional nitrogen sink in forested subtropical catchments (Yu et al., 2019).

4.2 | Dynamics of NO_3^- export and land cover

Contrary to $\delta^{18}O_{NO3}$, we found obvious correlations between both percentages of land cover (LC) and NO_3^- concentrations and $d^{15}N_{NO3}$, as well as between the two last themselves (Figure 5). This indicates that the changing land use resulted in increased NO_3^- concentrations what was likely attributed to the increasing contribution of MS, as this source is characterized by relatively high $\delta^{15}N_{NO3}$ and nutrient content. We excluded the possibility of increased $\delta^{15}N_{NO3}$ caused by the higher impact of denitrification because the correlation between $\delta^{18}O_{NO3}$ and $\delta^{15}N_{NO3}$ was insignificant. This is consistent with the concluded low impact of denitrification on a regional scale. Our findings align with the results of other studies involving stable isotopes in catchments characterized by high LC_{AGR} and LC_{URB}. For example, in

TABLE 1 Mean stable isotope and NO_3^- concentrations from surface water samples together with hydro-climatic indices calculated for event-based monitoring conducted in 2013. The corresponding *p* values calculated between pre-event and event sampling campaigns for measured parameters (NO_3^-, $\delta^{15}N_{NO3}$, $\delta^{18}O_{NO3}$, $\delta^{18}O_{H2O}$) are indicated by * ($p < 0.05$), ** ($p < 0.01$), as well as *** ($p < 0.001$); fields without any sign indicate $p > 0.05$. Mean precipitation calculated for the period between pre-event and event sampling campaign is shown in italic

Sampling campaigns			Hydro-climatic indices			Measured parameters				
Season	Time	Code[a]	Q_{total}[b] ($m^3\ s^{-1}$)	BFI[b] (–)	Quick Flow[b] ($m^3\ s^{-1}$)	Precipitation[c] ($mm\ day^{-1}$)	NO_3^- ($mg\ L^{-1}$)	$\delta^{15}N_{NO3}$ (‰) AIR	$\delta^{18}O_{NO3}$ (‰) VSMOW	$\delta^{18}O_{H2O}$ (‰) VSMOW
Winter	Pre-event	S5[d]	13.2	0.99	0.1	1.5 (±1.5) *28.7 (±6.2)*	3.9 (±1.5, $n = 15$)	1.4 (±2.8, $n = 15$)	−1.3 (±2.1, $n = 15$)	−10.67 (±0.52, $n = 15$)
	Event	S5A	125.3	0.10	112.2	18.0 (±5.7)	3.7 (±1.4, $n = 15$)	−0.3 (±1.3, $n = 15$)	5.0 (±3.2, $n = 15$)***	−12.04 (±0.61, $n = 15$)***
Spring	Pre-event	S6[d]	20.4	0.92	1.7	0.3 (±0.6) *1.4 (±0.8)*	4.8 (±1.9, $n = 8$)	1.4 (±3.0, $n = 8$)	4.4 (±1.9, $n = 8$)	−11.44 (±0.3, $n = 8$)
	Event	S6A	31.4	0.70	9.3	1.7 (±0.9)	4.8 (±1.8, $n = 8$)	0.4 (±1.7, $n = 8$)	6.5 (±2.1, $n = 8$)*	−11.86 (±0.37, $n = 8$)*
Summer	Pre-event	S8[d]	6.8	0.98	0.1	16.3 (±7.8) *7.2 (±3.8)*	5.1 (±2.8, $n = 11$)	1.7 (±2.8, $n = 11$)	2.9 (±1.5, $n = 11$)	−10.68 (±0.53, $n = 11$)
	Event	S8A	7.8	0.85	1.2	1.7 (±3.7)	5.2 (±2.6, $n = 11$)	2.1 (±1.9, $n = 11$)	0.9 (±2.9, $n = 11$)	−10.65 (±0.4, $n = 11$)
Autumn	Pre-event	S9[d]	7.4	0.89	0.9	5.0 (±5.0) *21.7(±6.9)*	4.0 (±1.6, $n = 11$)	2.7 (±2.9, $n = 11$)	4.7 (±2.2, $n = 11$)	−10.58 (±0.77, $n = 11$)
	Event	S9A	32.6	0.21	25.8	8.3 (±3.7)	4.1 (±1.1, $n = 11$)	0.6 (±2.3, $n = 11$)	4.8 (±2.3, $n = 11$)	−10.46 (±0.8, $n = 11$)

[a]Details about the sampling locations can be found in SI, Table 1.
[b]Calculated at the outlet (sampling location E19).
[c]Mean value calculated from the precipitation gauging stations located within the catchment and neighbourhoods.
[d]For comparability, only sampling locations included in subsequent event-based sampling campaign were taken into account.

their meta-analysis of 33 river catchments, Johannsen et al. (2008) found a strong positive correlation ($R^2 = 0.71$) between $\delta^{15}N_{NO3}$ values and the proportion of arable and urban land caused by increased inputs of nitrate from sewage and manure.

The presence of a strong correlation between Q_{spec} and SL_{NO3}, not observed between both percentages of LC and SL_{NO3}, suggests that Q_{spec} plays a more important role than LC in controlling SL_{NO3}. Both percentages of LC were also weakly correlated with Q_{spec}, with lower Q_{spec} found in sub-catchments with higher LC_{AGR}. This is likely to be related to the fact that most of the catchments with the highest LC_{AGR} are located on lower altitudes and receiving less precipitation than the mountainous sub-catchments.

4.2.1 | Spatiotemporal variations in proportional contributions of NO_3^- sources

The main source of NO_3^- along the main river and in forested catchments was RNS. The estimated proportional contributions of anthropogenic nitrate sources (MS and NF) were generally increasing along the main river during different seasons. Notably, the contribution of MS estimated by the model for the catchments characterized by a high LC_{AGR} and LC_{URB} was much higher than in forested sub-catchments. The proportional contribution of NF was relatively stable over the year in all sub-catchments, with generally slightly higher values in November. The application of fertilizers occurs mainly in the spring and fall seasons. In November, the N-uptake of the vegetation is significantly reduced, and some fields are left with no vegetation cover at all. Therefore, the washout of freshly applied fertilizers could be responsible for the higher contribution of NF in November. The proportional contribution of AD was low in all locations, with mean values not exceeding a few percent and not exhibiting any considerable changes over the year. The results show that most of the nitrate originating from AD is not contributing directly to the stream water, but it is processed through the biota and then nitrified before entering the stream. Many other studies that used stable isotopes in forested catchments report low proportional contribution (mean ~10%) of nitrate from atmospheric deposition contributing to streams during baseflow (Rose et al., 2015).

4.2.2 | Spatiotemporal variations in NO_3^- loads and their sources

The highest SL_{NO3} were found for the two campaigns with relatively high discharges (Figure 7, columns 1 and 2) emphasizing the importance of Q_{spec} role in controlling SL_{NO3}. The analysis of the SL_{NO3} derived from each of the four sources (Figure 7, rows 2–5) suggests that in catchments characterized by higher LC_{AGR}, especially those characterized by a high percentage of arable land, higher total SL_{NO3} were mainly related with increased SL_{NO3} derived from MS but also from NF. Very low SL_{NO3} derived from AD were related to

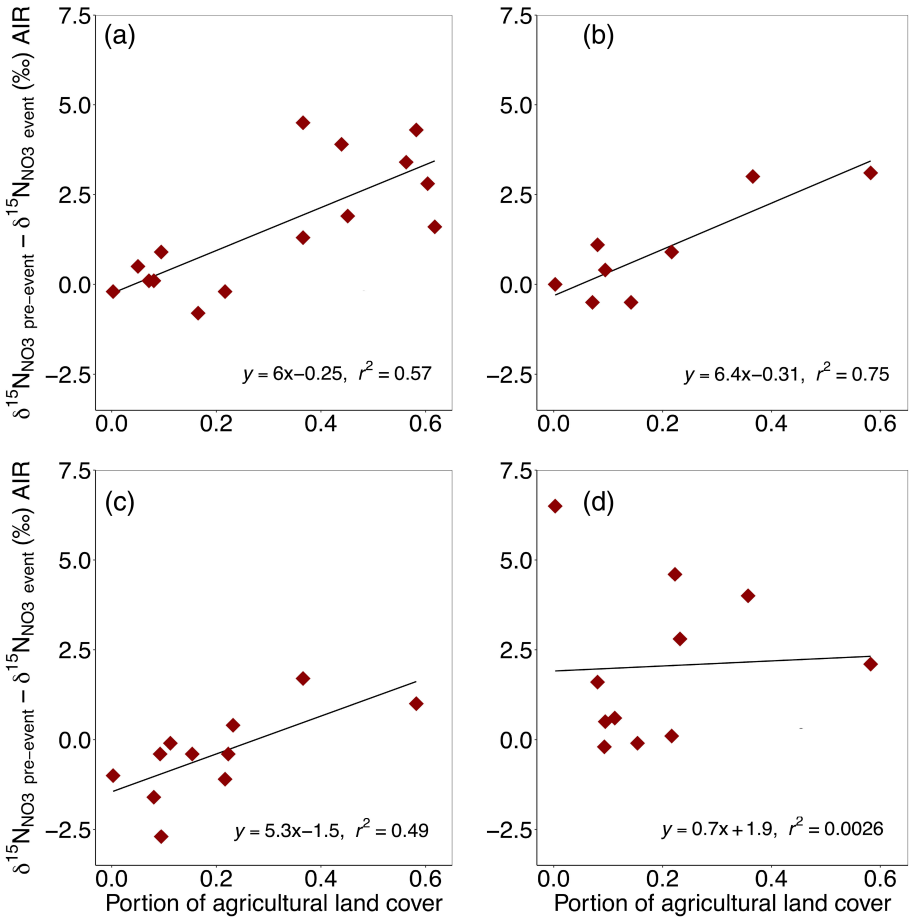

FIGURE 8 Linear correlations between the portions of the agricultural land cover and the difference in $\delta^{15}N_{NO3}$ values measured during the pre-event and event sampling campaigns in the respective sub-catchments for four investigated rainfall-runoff events. Figures present the data collected during pre-event and subsequent event-based monitoring campaigns conducted in winter (a), spring (b), summer (c), and autumn (d) 2013

the fact that sampling campaigns were performed when the base flow was the main component of total flow. Spatiotemporal patterns of SL_{NO3} derived from RNS suggest a preferred mobilization of the RNS source during periods of higher discharge.

4.3 | Dynamics of NO_3^- export and hydrological conditions

4.3.1 | Catchment response to rainfall-runoff events constrained by event-based monitoring

The lack of significant differences in mean NO_3^- concentrations and $\delta^{15}N_{NO3}$ between pre-event and event-based sampling campaigns (Table 1) is consistent with our previous finding that denitrification has a low impact in the investigated catchment on a regional scale. Moreover, no significant difference in mean NO_3^- concentrations suggests a low direct contribution of AD into the stream water and a low impact of dilution during event-based campaigns.

The observed significant differences between mean $\delta^{18}O_{NO3}$ and $\delta^{18}O_{H2O}$ measured during winter and spring event-based sampling campaigns and antecedent pre-event sampling campaigns are likely to be related to the change of water pathways. In the winter event-based campaign (S5A), the observed discharge at the outlet was several times higher than the mean discharge. In the spring event-based campaign (S6A), the observed discharge at the outlet was about double the mean discharge. During both winter and spring pre-event sampling campaigns, the mean precipitation was very low. The total discharge calculated at the outlet for the spring pre-event sampling campaign was higher than the mean discharge, indicating that the catchment was relatively wet. Observed higher $\delta^{18}O_{NO3}$ cannot be solely explained by the increased contribution of AD because they were not accompanied by a considerable drop in NO_3^- concentrations. Moreover, the measured mean nitrate isotopes values were typical for the RNS source. Additionally, runoff separation performed for both events revealed the increased contribution of quick flow. Therefore, the shifts in stable O isotopes of water and nitrate during winter and spring event-based monitoring are likely to be related to the change of water pathways. Due to the increased contribution of interflow (as one significant component of the quick flow), nitrate pools from the unsaturated zone could be mobilized. Mobilization of nitrate pools with elevated $\delta^{18}O_{NO3}$ from the unsaturated zone and the minor impact of the increased direct contribution of AD could explain the observed changes in the isotopic signatures during the investigated winter and spring events.

During summer and autumn rainfall-runoff events, we neither detected a significant difference for $\delta^{18}O_{NO3}$ nor $\delta^{18}O_{H2O}$. In summer, the pre-event sampling campaign (S8) was characterized by a total

discharge lower than half the mean discharge. Moreover, even though the precipitation was higher than during the spring event, both total discharge and quick flow increased to a small extend only. Those two facts indicate that antecedent to the event, the catchment was relatively dry. A low increase in the contribution of quick flow was likely to be responsible for the absence of a significant difference between mean $\delta^{18}O_{NO3}$ and $\delta^{18}O_{H2O}$ values measured during the summer pre-event and event sampling campaigns. In autumn, even though the BFI decreased noticeably between the pre-event and the event-based sampling campaign, a significant difference was not detected for any of the parameters. This might be related to the fact that the pre-event sampling campaign was not performed during pure base flow conditions (BFI = 0.89). Because interflow and surface runoff flow paths were already contributing to the streamflow during the pre-event sampling campaign, nitrate pools from the unsaturated zone were already mobilized at that time, and no significant difference in nitrate isotopes was observed. We expect that this different NO_3^- response to the rainfall-runoff events may be related to the antecedent conditions.

4.3.2 | Land-use control on sub-catchment responses to rainfall-runoff events

We further explored how different sub-catchments reacted to the rainfall-runoff events (Figure 8) by comparing the LC_{AGR} and the difference between $\delta^{15}N_{NO3}$ measured during a pre-event and an event sampling campaign. Correlations calculated between the percentage of LC and the differences in $\delta^{15}N_{NO3}$ measured during pre-event and event sampling campaigns (Figure 8) cannot be explained by the typical SD of $\delta^{15}N_{NO3}$. It is because SD of $\delta^{15}N_{NO3}$ shows lower values and does not follow the land cover gradient (Figure 3). The observed correlations between LC_{AGR} and event-related N-isotope shifts further confirm that the mobilization of RNS during precipitation events is driving the changes in $\delta^{15}N_{NO3}$, especially in the agricultural catchments where the MS contribution is high (see Figure 6). Stable isotope signatures imply that agricultural and forested catchments react differently to the rainfall-runoff events with respect to changes in pathways of nitrate pool mobilization. Lack of correlation between the LC_{AGR} and the difference between $\delta^{15}N_{NO3}$ measured during autumn pre-event and event sampling campaigns (Figure 8d) is likely related to the fact that the pre-event sampling campaign was not performed during pure base flow conditions (BFI = 0.89) and that the interflow and surface runoff flow paths were already contributing to the streamflow during the pre-event sampling campaign.

4.3.3 | Relationship between discharge, NO_3^- isotopic signatures, and NO_3^- export through the monitoring period

The results of the pairwise Spearman's correlation analysis between Q_{spec}, $\delta^{18}O_{NO3}$, and NO_3^- concentrations (Figure 5) indicate a low impact of dilution during periods of higher specific discharge in the investigated catchments. Considering the correlation between Q_{spec} and $\delta^{15}N_{NO3}$, one can conclude that periods of higher specific discharge in the investigated catchment are likely to be associated with a higher contribution of RNS or NF sources rather than a direct contribution of AD. Stronger correlations between SL_{NO3} and Q_{spec} compared to the correlation between SL_{NO3} and NO_3^- concentrations emphasize the impact of discharge changes on NO_3^- export from catchments.

Results of the correlation analysis between BFI and nitrate concentrations and isotopes (Table S6) support the assumption that nitrate pools with elevated $\delta^{18}O_{NO3}$ are mobilized from the unsaturated zone. We found that during the performed sampling campaigns, most of the atmospheric nitrate was not contributing directly to the stream. Instead, it was first cycled through the biota and fixed in the soil storage before it was nitrified and released to the stream. Our findings are consistent with the observations of Burns and Kendall (2002), who report a major contribution of atmospheric nitrate only during high flow events that exceeded the annual flow. None of the rainfall-runoff events investigated in our study exceed the annual flow. Moreover, our results suggest that different nitrate export pathways occur during different hydrological conditions.

5 | CONCLUSIONS

Our integrated approach provides valuable insights into the nitrate export from a mesoscale river catchment and its main controls: land-use, hydrological, and nitrate transformation processes. The studied Erlauf catchment is a typical representative of a mesoscale Alpine foothill catchment characterized by a land-use gradient from forested headwaters to agricultural lowlands. Therefore, our site-specific findings may be utilized to improve the interpretation of the data from low spatial resolution water quality monitoring in catchments with similar characteristics. In the Erlauf river system, nitrate from external sources is stored and accumulated in soil storage pools instead of being directly mobilized and dislocated. Nitrification of reduced nitrogen species in those pools plays the most important role for the N-dynamics in the study catchment. Consequently, nitrification of reduced N sources was the main nitrate source except for agricultural sub-catchments. In this study, land use is the important driver of nitrate export. The agricultural land cover was tied to elevated nitrate concentrations and changes in the proportional contribution of nitrate sources, especially a significantly higher contribution of manure and sewage. In the Erlauf catchment, nitrate degradation potential is not high enough to solely control nitrate export, and on a regional scale, denitrification plays only a minor role. Therefore, high specific nitrate loads in small agricultural catchments may only be managed by reducing the nitrogen surplus. One option would be the utilization of precision farming techniques allowing a spatially distributed application of organic and chemical fertilizers according to the actual fertilization demand.

ACKNOWLEDGEMENTS

We thank Martina Neuber, Silke Köhler, Petra Blümel and Wolfgang Städter for running numerous chemical and isotope analyses. This project has received funding from the European Union's Horizon 2020 research and innovation programme under the Marie Skłodowska-Curie grant agreement No. 675120 (ITN INSPIRATION).

DATA AVAILABILITY STATEMENT

The data that support the findings of this study are available from the corresponding author upon reasonable request.

ORCID

Izabela Bujak https://orcid.org/0000-0002-3059-7376

REFERENCES

Aravena, R., & Robertson, W. D. (1998). Use of multiple isotope tracers to evaluate denitrification in ground water. Study of nitrate from a large-flux septic system plume. *Ground Water*, *36*(6), 975–982. https://doi.org/10.1111/j.1745-6584.1998.tb02104.x

Bateman, A. S., & Kelly, S. D. (2007). Fertilizer nitrogen isotope signatures. *Isotopes in Environmental and Health Studies*, *43*(3), 237–247.

Bishop, K., Buffam, I., Erlandsson, M., Fölster, J., Laudon, H., Seibert, J., & Temnerud, J. (2008). Aqua incognita: The unknown headwaters. *Hydrological Processes*, *22*, 1239–1242.

Blöschl, G., Blaschke, A. P., Broer, M., Bucher, C., Carr, G., Chen, X., Eder, A., Exner-Kittridge, M., Farnleitner, A., Flores-Orozco, A., Haas, P., Hogan, P., Kazemi Amiri, A., Oismüller, M., Parajka, J., Silasari, R., Stadler, P., Strauss, P., Vreugdenhil, M., … Zessner, M. (2016). The hydrological open air laboratory (HOAL) in Petzenkirchen. A hypothesis-driven observatory. *Hydrology and Earth System Sciences*, *20*(1), 227–255.

BMLFUW (2014): Flächenverzeichnis der Flussgebiete: Donaugebiet von der Enns bis zur Leitha. Beiträge zur Hydrografie Österreichs Heft 62. Bundesministerium Für Land- Und Forstwirtschaft, Umwelt Und Wasserwirtschaft. Wien. https://www.bmnt.gv.at/wasser/wasser-oesterreich/wasserkreislauf/einzugsgebiete2012.html.

Braun, B., & Schagerl, M. (2010). Algae-environment relationships in an impoundment stretch of the river Grosse Erlauf (Austria). *River Systems*, *19*(1), 3–13.

Burns, D. A., & Kendall, C. (2002). Analysis of δ15N and δ18O to differentiate NO3− sources in runoff at two watersheds in the Catskill Mountains of New York. *Water Resources Research*, *38*(5), 9–1.

Casciotti, K. L., Sigman, D. M., Hastings, M. G., Böhlke, J. K., & Hilkert, A. (2002). Measurement of the oxygen isotopic composition of nitrate in seawater and freshwater using the denitrifier method. *Analytical chemistry*, *74*(19), 4905–4912.

Casciotti, K. L., & Buchwald, C. (2012). Insights on the marine microbial nitrogen cycle from isotopic approaches to nitrification. *Frontiers in Microbiology*, *3*, 356. https://doi.org/10.3389/fmicb.2012.00356

Curt, M. D., Aguado, P., Sanchez, G., Bigeriego, M., & Fernández, J. (2004). Nitrogen isotope ratios of synthetic and organic sources of nitrate water contamination in Spain. *Water, Air, and Soil Pollution*, *151*(1–4), 135–142.

Deutsch, B., Kahle, P., & Voss, M. (2006). Assessing the source of nitrate pollution in water using stable N and O isotopes. *Agronomy for Sustainable Development*, *26*(4), 263–267.

Ding, J., Xi, B., Gao, R., He, L., Liu, H., Dai, X., & Yu, Y. (2014). Identifying diffused nitrate sources in a stream in an agricultural field using a dual isotopic approach. *The Science of the Total Environment*, *484*, 10–18. https://doi.org/10.1016/j.scitotenv.2014.03.018

Divers, M. T., Elliott, E. M., & Bain, D. J. (2014). Quantification of nitrate sources to an urban stream using dual nitrate isotopes. *Environmental Science & Technology*, *48*(18), 10580–10587.

EEA. (2012). Land Cover: European Environment Agency.

EU. (2000). *Directive 2000/60/EC of the European Parliament and of the council of 23 October 2000 establishing a framework for community action in the field of water policy water framework directive*. Water Framework Directive.

Fogg, G. E., Rolston, D. E., Decker, D. L., Louie, D. T., & Grismer, M. E. (1998). Spatial variation in nitrogen isotope values beneath nitrate contamination sources. *Ground Water*, *36*(3), 418–426. https://doi.org/10.1111/j.1745-6584.1998.tb02812.x

Fukada, T., Hiscock, K. M., Dennis, P. F., & Grischek, T. (2003). A dual isotope approach to identify denitrification in groundwater at a river-bank infiltration site. *Water Research*, *37*(13), 3070–3078.

GBA (2020). Geologischen Bundesanstalt (GBA). Geological Map of Austria 1:500000. https://www.geologie.ac.at/services/web-services/.

Gröning, M., Lutz, H. O., Roller-Lutz, Z., Kralik, M., Gourcy, L., & Pöltenstein, L. (2012). A simple rain collector preventing water re-evaporation dedicated for δ18O and δ2H analysis of cumulative precipitation samples. *Journal of Hydrology*, *448*, 195–200.

Harms, T. K., & Grimm, N. B. (2008). Hot spots and hot moments of carbon and nitrogen dynamics in a semiarid riparian zone. *Journal of Geophysical Research*, *113*, 1–14. https://doi.org/10.1029/2007JG000588

Heaton, T. H. E. (1986). Isotopic studies of nitrogen pollution in the hydrosphere and atmosphere. A review. *Chemical Geology*, *59*(1), 87–102.

Institute of Hydrology. (1980). *Low Flow Studies*, *Report 1*. Institute of Hydrology.

Jin, Z., Zheng, Q., Zhu, C., Wang, Y., Cen, J., & Li, F. (2018). Contribution of nitrate sources in surface water in multiple land use areas by combining isotopes and a Bayesian isotope mixing model. *Applied Geochemistry*, *93*, 10–19.

Johannsen, A., Dähnke, K., & Emeis, K. (2008). Isotopic composition of nitrate in five German rivers discharging into the North Sea. *Organic Geochemistry*, *39*(12), 1678–1689.

Kendall, C., Elliott, E. M., & Wankel, S. D. (2007). Tracing anthropogenic inputs of nitrogen to ecosystems. *Stable Isotopes in Ecology and Environmental Science*, *2*, 375–449.

Kendall, C., & McDonnell, J. J. (1998). *Isotope tracers in catchment hydrology*. Elsevier.

Kohl, D. H., Shearer, G. B., & Commoner, B. (1971). Fertilizer nitrogen. Contribution to nitrate in surface water in a corn belt watershed. *Science*, *174*(4016), 1331–1334.

Kool, D. M., Wrage, N., Oenema, O., van Kessel, C., & van Groenigen, J. W. (2011). Oxygen exchange with water alters the oxygen isotopic signature of nitrate in soil ecosystems. *Soil Biology and Biochemistry*, *43*(6), 1180–1185.

Kreitler, C. W., & Browning, L. A. (1983). Nitrogen-isotope analysis of groundwater nitrate in carbonate aquifers. Natural sources versus human pollution. *Journal of Hydrology*, *61*(1–3), 285–301. https://doi.org/10.1016/0022-1694(83)90254-8

Land Kärnten (2015). Digital Elevation Model (DEM). https://www.data.gv.at/katalog/dataset/b5de6975-417b-4320-afdb-eb2a9e2a1dbf.

Lark, R. M. (2000). A comparison of some robust estimators of the variogram for use in soil survey. *European Journal of Soil Science*, *51*(1), 137–157.

Lee, K.-S., Bong, Y.-S., Lee, D., Kim, Y., & Kim, K. (2008). Tracing the sources of nitrate in the Han River watershed in Korea, using δ15N-NO3− and δ18O-NO3− values. *Science of the Total Environment*, *395*(2–3), 117–124.

Li, C., Li, S.-L., Yue, F.-J., Liu, J., Zhong, J., Yan, Z.-F., Zhang, R.-C., Wang, Z.-J., & Xu, S. (2019). Identification of sources and transformations of nitrate in the Xijiang River using nitrate isotopes and Bayesian model. *Science of the Total Environment*, *646*, 801–810.

Li, X., Masuda, H., Koba, K., & Zeng, H. (2007). Nitrogen isotope study on nitrate-contaminated groundwater in the Sichuan Basin, China. *Water, Air, and Soil Pollution*, *178*(1–4), 145–156.

Lintern, A., McPhillips, L., Winfrey, B., Duncan, J., & Grady, C. (2020). Best management practices for diffuse nutrient pollution: Wicked problems across urban and agricultural watersheds. *Environmental Science & Technology*, *54*(15), 9159–9174.

Liu, C.-Q., Li, S.-L., Lang, Y.-C., & Xiao, H.-Y. (2006). Using δ 15 N- and δ 18 O-values to identify nitrate sources in karst ground water, Guiyang, Southwest China. *Environmental Science & Technology*, *40*(22), 6928–6933. https://doi.org/10.1021/es0610129

Mariotti, A., Landreau, A., & Simon, B. (1988). 15N isotope biogeochemistry and natural denitrification process in groundwater. Application to the chalk aquifer of northern France. *Geochimica et Cosmochimica Acta*, *52*(7), 1869–1878.

Mayer, B., Bollwerk, S. M., Mansfeldt, T., Hütter, B., & Veizer, J. (2001). The oxygen isotope composition of nitrate generated by nitrification in acid forest floors. *Geochimica et Cosmochimica Acta*, *65*(16), 2743–2756. https://doi.org/10.1016/S0016-7037(01)00612-3

McAleer, E. B., Coxon, C. E., Richards, K. G., Jahangir, M. M. R., Grant, J., & Mellander, P. E. (2017). Groundwater nitrate reduction versus dissolved gas production. A tale of two catchments. *Science of the Total Environment*, *586*, 372–389.

Mengis, M., Schif, S. L., Harris, M., English, M. C., Aravena, R., Elgood, R. J., & MacLean, A. (1999). Multiple geochemical and isotopic approaches for assessing ground water NO3- elimination in a riparian zone. *Ground Water*, *37*(3), 448–457. https://doi.org/10.1111/j.1745-6584.1999.tb01124.x

Merz, R., Blöschl, G., & Humer, G. (2008). National flood discharge mapping in Austria. *Natural Hazards*, *46*, 53–72.

Moore, J. W., & Semmens, B. X. (2008). Incorporating uncertainty and prior information into stable isotope mixing models. *Ecology Letters*, *11*(5), 470–480. https://doi.org/10.1111/j.1461-0248.2008.01163.x

Mueller, C., Krieg, R., Merz, R., & Knöller, K. (2016). Regional nitrogen dynamics in the TERENO Bode River catchment, Germany, as constrained by stable isotope patterns. *Isotopes in Environmental and Health Studies*, *52*(1–2), 61–74. https://doi.org/10.1080/10256016.2015.1019489

Mueller, C., Zink, M., Samaniego, L., Krieg, R., Merz, R., Rode, M., & Knöller, K. (2016). Discharge driven nitrogen dynamics in a mesoscale river basin as constrained by stable isotope patterns. *Environmental Science & Technology*, *50*(17), 9187–9196.

Nash, J. E., & Sutcliffe, J. V. (1970). River flow forecasting through conceptual models part I—A discussion of principles. *Journal of Hydrology*, *10*(3), 282–290.

Nestler, A., Berglund, M., Accoe, F., Duta, S., Xue, D., Boeckx, P., & Taylor, P. (2011). Isotopes for improved management of nitrate pollution in aqueous resources. Review of surface water field studies. *Environmental Science and Pollution Research*, *18*(4), 519–533.

NÖ. (2019). Wasserstandsnachrichten und Hochwasserprognosen. NÖ Landesregierung. https://www.noe.gv.at/wasserstand/#/de/Messstellen/.

OIEau. (2019). Urban Waste Water Treatment Directive (UWWTD) site for Austria. Office International de l'Eau. https://uwwtd.eu/Austria/.

Palta, M. M., Ehrenfeld, J. G., & Groffman, P. M. (2014). "Hotspots" and "hot moments" of denitrification in urban brownfield wetlands. *Ecosystems*, *17*(7), 1121–1137. https://doi.org/10.1007/s10021-014-9778-0

Panno, S. V., Hackley, K. C., Kelly, W. R., & Hwang, H.-H. (2006). Isotopic evidence of nitrate sources and denitrification in the Mississippi River, Illinois. *Journal of Environmental Quality*, *35*(2), 495–504. https://doi.org/10.2134/jeq2005.0012

Panno, S. V., Kelly, W. R., Hackley, K. C., Hwang, H.-H., & Martinsek, A. T. (2008). Sources and fate of nitrate in the Illinois River basin, Illinois. *Journal of Hydrology*, *359*(1–2), 174–188. https://doi.org/10.1016/j.jhydrol.2008.06.027

Parajka, J., Merz, R., Skøien, J. O., & Viglione, A. (2015). The role of station density for predicting daily runoff by top-kriging interpolation in Austria. *Journal of Hydrology and Hydromechanics*, *63*(3), 228–234. https://doi.org/10.1515/johh-2015-0024

Parnell, A. C., Inger, R., Bearhop, S., & Jackson, A. L. (2010). Source partitioning using stable isotopes. Coping with too much variation. *PLoS One*, *5*(3), e9672.

Peter, S., Rechsteiner, R., Lehmann, M. F., Tockner, K., Vogt, T., Wehrli, B., & Durisch-Kaiser, E. (2011). Denitrification hot spot and hot moments in a restored riparian system. In *Gq10: Groundwater quality management in a rapidly changing world* (pp. 433–436). International Association of Hydrological Sciences.

R Core Team (2018): R. A language and environment for statistical computing. http://www.R-project.org/.

Rapisarda, P., Camin, F., Fabroni, S., Perini, M., Torrisi, B., & Intrigliolo, F. (2010). Influence of different organic fertilizers on quality parameters and the $\delta^{15}N$, $\delta^{13}C$, $\delta^{2}H$, $\delta^{34}S$, and $\delta^{18}O$ values of orange fruit (*Citrus sinensis* L. Osbeck). *Journal of Agricultural and Food Chemistry*, *58*(6), 3502–3506. https://doi.org/10.1021/jf903952v

Rennie, D. A., Paul, E. A., & Johns, L. E. (1976). Natural Nitrogen-15 abundance of soil and plant samples. *Canadian Journal of Soil Science*, *56*(1), 43–50. https://doi.org/10.4141/cjss76-006

Rogers, K. M. (2008). Nitrogen isotopes as a screening tool to determine the growing regimen of some organic and nonorganic supermarket produce from New Zealand. *Journal of Agricultural and Food Chemistry*, *56*(11), 4078–4083. https://doi.org/10.1021/jf800797w

Rose, L. A., Sebestyen, S. D., Elliott, E. M., & Koba, K. (2015). Drivers of atmospheric nitrate processing and export in forested catchments. *Water Resources Research*, *51*(2), 1333–1352.

Schlesinger, W. H., Reckhow, K. H., & Bernhardt, E. S. (2006). Global change. The nitrogen cycle and rivers. *Water Resources Research*, *42*(3), 758. https://doi.org/10.1029/2005WR004300

Schumacher. (2016). EU takes Germany to court over environmental standards.

Schwientek, M., Osenbrück, K., & Fleischer, M. (2013). Investigating hydrological drivers of nitrate export dynamics in two agricultural catchments in Germany using high-frequency data series. *Environmental Earth Sciences*, *69*(2), 381–393.

Sebilo, M., Billen, G., Mayer, B., Billiou, D., Grably, M., Garnier, J., & Mariotti, A. (2006). Assessing nitrification and denitrification in the Seine River and estuary using chemical and isotopic techniques. *Ecosystems*, *9*(4), 564–577. https://doi.org/10.1007/s10021-006-0151-9

Sigman, D. M., Casciotti, K. L., Andreani, M., Barford, C., Galanter, M. B. J. K, & Böhlke, J. K. (2001). A bacterial method for the nitrogen isotopic analysis of nitrate in seawater and freshwater. *Analytical chemistry*, *73*(17), 4145–4153.

Skøien, J. O., Blöschl, G., Laaha, G., Pebesma, E., Parajka, J., & Viglione, A. (2014). Rtop. An R package for interpolation of data with a variable spatial support, with an example from river networks. *Computers & Geosciences*, *67*, 180–190. https://doi.org/10.1016/j.cageo.2014.02.009

Skøien, J. O., Merz, R., & Blöschl, G. (2006). Top-kriging-geostatistics on stream networks. *Hydrology and Earth System Sciences*, *10*(2), 277–287. https://doi.org/10.5194/hess-10-277-2006

Skøien, J. O., & Blöschl, G. (2007). Spatiotemporal topological kriging of runoff time series. *Water Resources Research*, *43*(9), 2061. https://doi.org/10.1029/2006WR005760

Soulsby, C., Petry, J., Brewer, M. J., Dunn, S. M., Ott, B., & Malcolm, I. A. (2003). Identifying and assessing uncertainty in hydrological pathways. A novel approach to end member mixing in a Scottish agricultural catchment. *Journal of Hydrology*, *274*(1–4), 109–128. https://doi.org/10.1016/S0022-1694(02)00398-0

Spoelstra, J., Schiff, S. L., Hazlett, P. W., Jeffries, D. S., & Semkin, R. G. (2007). The isotopic composition of nitrate produced from nitrification in a hardwood forest floor. *Geochimica et Cosmochimica Acta*, *71*(15), 3757–3771. https://doi.org/10.1016/j.gca.2007.05.021

Stock, B. C., Jackson, A. L., Ward, E. J., Parnell, A. C., Phillips, D. L., & Semmens, B. X. (2018). Analyzing mixing systems using a new generation of Bayesian tracer mixing models. *PeerJ*, *6*, e5096.

Strauss (2009): River Erlauf, Austria. PEER Partnership for European Environmental Research.

Van Meerveld, H. J., Sauquet, E., Gallart, F., Sefton, C., Seibert, J., & Bishop, K. (2020). Aqua temporaria incognita. *Hydrological Processes*, *34*, 5704–5711.

Vitòria, L., Otero, N., Soler, A., & Canals, À. (2004). Fertilizer characterization: Isotopic data (N, S, O, C, and Sr). *Environmental Science & Technology*, *38*(12), 3254–3262.

von Schiller, D., Bernal, S., Dahm, C. N., & Martí, E. (2017). Nutrient and organic matter dynamics. In *Intermittent Rivers and Ephemeral Streams* (pp. 135–160). Academic Press. https://doi.org/10.1016/B978-0-12-803835-2.00006-1

Voss, M., Deutsch, B., Elmgren, R., Humborg, C., Kuuppo, P., Pastuszak, M., Rolff, C., & Schulte, U. (2006). Source identification of nitrate by means of isotopic tracers in the Baltic Sea catchments. *Biogeosciences*, *3*(4), 663–676. https://doi.org/10.5194/bg-3-663-2006

Vrzel, J., Vuković-Gačić, B., Kolarević, S., Gačić, Z., Kračun-Kolarević, M., Kostić, J., Aborgiba, M., Farnleitner, A., Reischer, G., Linke, R., Paunović, M., & Ogrinc, N. (2016). Determination of the sources of nitrate and the microbiological sources of pollution in the Sava River basin. *Science of the Total Environment*, *573*, 1460–1471.

Wall, D., Jordan, P., Melland, A. R., Mellander, P.-E., Buckley, C., Reaney, S. M., & Shortle, G. (2011). Using the nutrient transfer continuum concept to evaluate the European Union nitrates directive National Action Programme. *Environmental Science & Policy*, *14*(6), 664–674.

Wassenaar, L. I. (1995). Evaluation of the origin and fate of nitrate in the Abbotsford aquifer using the isotopes of15N and18O in NO3−. *Applied Geochemistry*, *10*(4), 391–405.

WHO, & Edition, F. (2011). Guidelines for drinking-water quality. *WHO Chronicle*, *38*(4), 104–108.

Widory, D., Petelet-Giraud, E., Négrel, P., & Ladouche, B. (2005). Tracking the sources of nitrate in groundwater using coupled nitrogen and boron isotopes. A Synthesis. *Environmental Science & Technology*, *39*(2), 539–548. https://doi.org/10.1021/es0493897

Williard, K. W. J., DeWalle, D. R., Edwards, P. J., & Sharpe, W. E. (2001). 18O isotopic separation of stream nitrate sources in mid-Appalachian forested watersheds. *Journal of Hydrology*, *252*(1–4), 174–188.

Xia, Y., Li, Y., Zhang, X., & Yan, X. (2017). Nitrate source apportionment using a combined dual isotope, chemical and bacterial property, and Bayesian model approach in river systems. *Journal of Geophysical Research: Biogeosciences*, *122*(1), 2–14. https://doi.org/10.1002/2016JG003447

Xing, M., & Liu, W. (2016). Using dual isotopes to identify sources and transformations of nitrogen in water catchments with different land uses, loess plateau of China. *Environmental Science and Pollution Research*, *23*(1), 388–401. https://doi.org/10.1007/s11356-015-5268-y

Xue, D., Botte, J., de Baets, B., Accoe, F., Nestler, A., Taylor, P., van Cleemput, O., Berglund, M., & Boeckx, P. (2009). Present limitations and future prospects of stable isotope methods for nitrate source identification in surface-and groundwater. *Water Research*, *43*(5), 1159–1170.

Xue, D., de Baets, B., van Cleemput, O., Hennessy, C., Berglund, M., & Boeckx, P. (2012). Use of a Bayesian isotope mixing model to estimate proportional contributions of multiple nitrate sources in surface water. *Environmental Pollution*, *161*, 43–49.

Yu, L., Mulder, J., Zhu, J., Zhang, X., Wang, Z., & Dörsch, P. (2019). Denitrification as a major regional nitrogen sink in subtropical forest catchments: Evidence from multi-site dual nitrate isotopes. *Global Change Biology*, *25*, 1765–1778.

Yue, F.-J., Li, S.-L., & Hu, J. (2015). The contribution of nitrate sources in Liao Rivers, China, based on isotopic fractionation and Bayesian mixing model. *Procedia Earth and Planetary Science*, *13*, 16–20.

Zhang, Y., Liu, X. J., Fangmeier, A., Goulding, K. T. W., & Zhang, F. S. (2008). Nitrogen inputs and isotopes in precipitation in the North China plain. *Atmospheric Environment*, *42*(7), 1436–1448.

Zhang, Y., Shi, P., Li, F., Wei, A., Song, J., & Ma, J. (2018). Quantification of nitrate sources and fates in rivers in an irrigated agricultural area using environmental isotopes and a Bayesian isotope mixing model. *Chemosphere*, *208*, 493–501. https://doi.org/10.1016/j.chemosphere.2018.05.164

SUPPORTING INFORMATION

Additional supporting information may be found in the online version of the article at the publisher's website.

How to cite this article: Bujak, I., Müller, C., Merz, R., & Knöller, K. (2021). High spatial-resolution monitoring to investigate nitrate export and its drivers in a mesoscale river catchment along an anthropogenic land-cover gradient. *Hydrological Processes*, *35*(12), e14361. https://doi.org/10.1002/hyp.14361